Macromolecules

ARTICLE

pubs.acs.org/Macromolecules

Aggregation of Ureido-Pyrimidinone Supramolecular Thermoplastic Elastomers into Nanofibers: A Kinetic Analysis

Wilco P. J. Appel,[†] Giuseppe Portale,[§] Eva Wisse,[†] Patricia Y. W. Dankers,[†] and E. W. Meijer*[,†]

[†]Institute for Complex Molecular Systems and Laboratory of Macromolecular and Organic Chemistry, Eindhoven University of Technology, P.O. Box 513, 5600 MB Eindhoven, The Netherlands

[§]Netherlands Organization for Scientific Research (NWO), European Synchrotron Radiation Facility (ESRF), DUBBLE-CRG, Grenoble, F-38043, France

Supporting Information

ABSTRACT: The self-complementary hydrogen bonding ureido-pyrimidinone (UPy) motif is widely used in the design of supramolecular polymers because of its high dimerization constant. Lateral aggregation into fibrous structures is achieved by the addition of urea functions close to the UPy end group of low-T_g oligomers, yielding supramolecular thermoplastic elastomers. The rate of fiber formation is critically dependent on the substituent at the five- and six-positions of the UPy unit. Here the aggregation behavior in the solid state is disclosed for a series of molecules with the commonly used methyl, the optically pure (*S*)-2,7-dimethylheptyl and (*S*)-1-methylpropyl, and the racemic 1-ethylpentyl group at the six-position. The rate of nanofiber crystallization from the melt was investigated with a variety of techniques, including SAXS, WAXS, AFM, DSC, IR, and CD spectroscopy. As a result, the different stages involved in the nanofiber formation were elucidated. The nanofiber formation is a hierarchical process starting from the phase-separated melt with the dimerization of the UPy-units. For the lateral aggregation into high aspect nanofibers, both a nonsubstituted five position and urea functionalities are required. The nanofiber formation is the result of 1D stack formation accompanied by secondary nucleation of multiple stacks. The stack-to-stack distance within a nanofiber is dependent on the size of the UPy-substituent, which demonstrates that the substituents are in-between the stacks in the nanofibers. The results also demonstrate that stack and nanofiber formation is slowed down and suppressed by a branching of the six-substituent close to the UPy motif, whereas the presence of stereochemical isomers further suppresses this aggregation from the melt. These detailed insights into the kinetic behavior of nanofiber formation pave the way to create adaptable supramolecular materials.

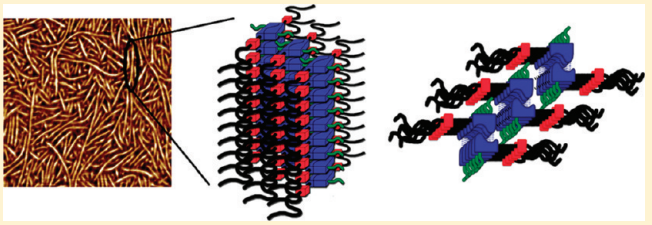

INTRODUCTION

The domain morphology of microphase separation between hard and soft domains in thermoplastic elastomers (TPEs) has been studied extensively.[1] TPEs based on hard domains as the result of hydrogen bonding are known to have intriguing properties, and the diversity of the hydrogen-bonding motifs allows for tunable morphologies. Recently, a number of hydrogen-bonded motifs are disclosed that possess nanofiber structures for the hard domains and yield materials with sharp thermal transitions. The evolution of synthetic macromolecules to supramolecular polymers has introduced a next generation of materials based on noncovalent interactions. Hydrogen bonding has been proven to be especially suitable as a noncovalent interaction for supramolecular synthesis because the direction of hydrogen bonds is more controlled than that of for instance ionic interactions.[2] Therefore, hydrogen-bonded supramolecular polymers hold promise as a unique class of novel materials because they combine many of the attractive features of conventional polymers with properties that result from the reversibility of the noncovalent bonds between the monomeric units.[3] Examples making use of the dynamic nature of the hydrogen bonding are found in advanced mechanical properties of biomimetic polymers[4] and the recombination of noncovalent bonds in self-healing materials.[5] Even TPEs are disclosed from supramolecular polymers.[6]

Because of the introduction of the strongly associating 2-ureido-4-pyrimidinone (UPy) motif as a quadruple hydrogen bonding moiety in telechelic supramolecular polymers,[7] numerous studies have been reported by us and others on its potential in supramolecular materials.[8] Because of the self-complementary motif and its high dimerization constant of 6×10^7 M^{-1} in $CHCl_3$,[9] a high degree of supramolecular polymerization can be achieved,[10] which transforms the macroscopic properties of the low-molecular-weight supramolecular monomer into those of a high-molecular-weight polymer.[6a] UPy-functionalization of telechelic oligomers based on poly(ethylene butylene),[6a] polystyrene,[11] polyesters,[12] polycarbonates,[13] polysiloxanes,[14] and polyethers[15] was reported to enhance the mechanical properties when compared with their unfunctionalized counterparts. In many cases, these mechanical properties are further

Received: June 9, 2011
Revised: August 1, 2011
Published: August 15, 2011

ACS Publications © 2011 American Chemical Society

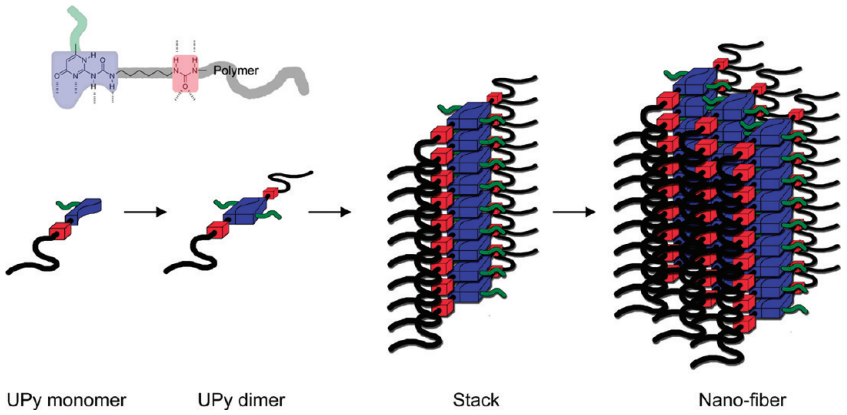

Figure 1. Schematic representation of the theoretical aggregation of the end groups of UPy (blue) urea (red)-modified polymers into nanofibers. The UPy-substituent at the six-position is depicted in green.

Chart 1. UPy-Urea Supramolecular Polymers 1−5 Used in This Study

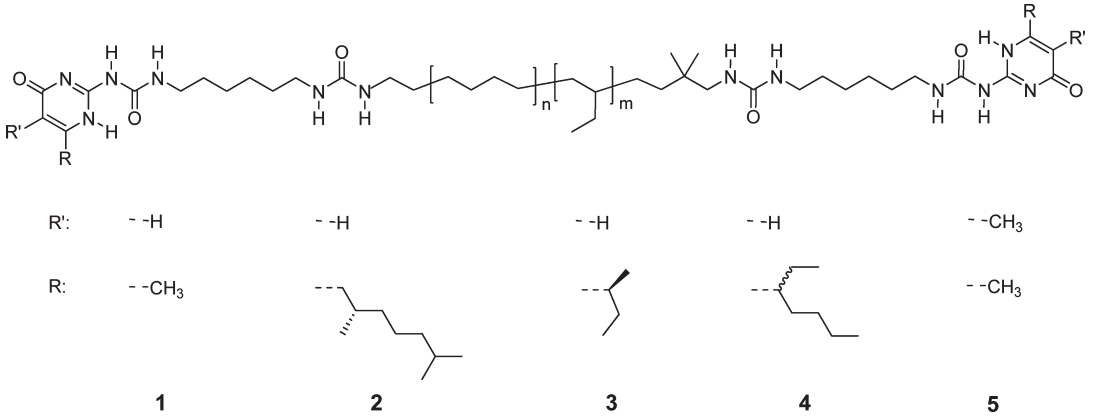

improved when the connecting group between the UPy moiety and the oligomer is a urethane or urea.[16]

In the case of low-T_g oligomers, the additional hydrogen bond that can be formed between the urea linker permits stacking of UPy dimers, which gives rise to TPEs. These materials show characteristic, well-defined nanofibers with a diameter of 6 to 7 nm, as observed with AFM.[16a] The nanofibrillar structure observed in the UPy-urea polymers shows close resemblance with the structure as observed in traditional TPEs or bisurea supramolecular polymers.[17]

We propose the formation of the UPy-urea nanofibers to be the result of a hierarchical process involving a number of steps, as illustrated in Figure 1.[16,17] The first step in the aggregation of the UPy-urea polymers is the dimerization of the UPy (depicted in blue), giving rise to the UPy dimers. This affords a bisurea unit that can self-assemble via lateral hydrogen bonding interactions (depicted in red). The resulting stacks subsequently form nanofibers, most probably via a secondary nucleation process. The aggregation of the UPy-urea moieties can induce phase segregation of the UPy-urea moieties from the polymer backbone, which will be an important driving force for the nanofiber formation.

The most frequently used UPy is derived from commercially available 6-methyl isocytosine,[6a] although different substituents on the six-position of the isocytosine have been reported.[14,18] The importance of the substituent at the six-position on the aggregation of UPy-urea based oligomers has not yet been systematically addressed. This is surprising because a detailed understanding of the structure−property relationship can provide tools for easy tuning of material properties.

A small library of bis-(UPy-urea) telechelic polymers with an amorphous poly(ethylene butylene) backbone was synthesized (Chart 1) in which the substituent changed from a methyl (**1**) to the optically pure (*S*)-2,7-dimethylheptyl (**2**) and (*S*)-1-methylpropyl (**3**) and the racemic 1-ethylpentyl (**4**) group. These selected groups permit us to investigate the influence of size, optical purity, and branching point on the aggregation of bis-(UPy-urea) polymers. Moreover, a 5,6-dimethyl UPy-urea polymer (**5**) was synthesized to evaluate the role of the substituent at the five-position. The hierarchical self-assembly of the UPy-urea moieties of polymers **1**−**5** was investigated by DSC, AFM, SAXS, WAXS, IR, UV−vis, and CD spectroscopy in the solid state and showed that the aggregation behavior on the molecular scale can be directly linked to their macroscopic properties.

EXPERIMENTAL SECTION

The synthesis and characterization of polymers **1**−**5** are described in the Supporting Information.

Differential Scanning Calorimetry. Differential scanning calorimetry (DSC) measurements were performed on a Thermal Advantage Q2000 apparatus between −80 and 150 °C at a rate of 10 K/min with a sample weight of 5−10 mg. The polymers were obtained by precipitation in acetone or methanol and were dried overnight at 40 °C in vacuo. For monitoring the nanofiber formation, the samples were heated 10 °C above the melting point and cooled back to 25 °C at 10 K/min and equilibrated for the given time prior to reheating. The materials were molten for a maximum of three times in a single experiment to exclude the influence of possible thermal degradation, after which a fresh batch of material was used for the additional experiments. Integration of the melting endotherm was performed with the TA Instruments Universal Analysis software.

Variable Temperature Atomic Force Microscopy. Atomic force microscopy (AFM) measurements were performed on a Digital Instrument Multimode Nanoscope IV operating in the tapping mode using silicon cantilever tips (PPP-NCH-50, 204−497 kHz, 10−130 N/m) with an amplitude set point of 2.0 V. Polymer films were made by casting a 1 mg/mL solution in chloroform on precleaned glass slides and subsequent evaporation to air for at least 1 h, followed by annealing in vacuo overnight at 40 °C. The polymer films were equilibrated at room temperature for at least 1 week prior to measurements.

Infrared Spectroscopy. Variable temperature infrared (IR) spectroscopy was performed on an Excalibur FTS 3000 MX equipped with a Golden Gate ATR setup with a resolution of 2 cm^{-1}. Fifty scans were accumulated after equilibrating for 2 min at the set temperature. The solid polymer films were made by dissolving the polymer in chloroform and evaporation to air for 4 h, followed by annealing in vacuo overnight at 40 °C. The polymer films were equilibrated at room temperature for at least 1 week prior to measurements.

Circular Dichroism Spectroscopy. Circulair dichroism (CD) spectra were recorded on a Jasco J815 spectrometer equipped with a Linkam hotstage. Polymers 1−4 were spin-cast from a 40 mg/mL solution in chloroform at 2000 rpm onto quartz glass slides to yield polymer films of ∼500 nm thick. The samples were allowed to equilibrate at the set temperature for 2 min prior to the measurement. Three scans were accumulated at a scanning speed of 20 nm/min.

UV−vis Absorption Spectroscopy. UV−vis absorption spectra were recorded on a Perkin-Elmer Lambda 900 spectrometer equipped with a Linkam hotstage. Measurements were performed as with CD spectroscopy.

X-ray Scattering. Small-angle X-ray scattering (SAXS) and wide-angle X-ray scattering (WAXS) experiments were performed on molten samples of at least 2 weeks old at the DUBBLE beamline (BM26B) at the European Synchrotron Radiation Facility (ESRF) in Grenoble (France). The materials were treated identical to the DSC crystallization experiments, that is, heated 10 °C above the melting point and cooled back to 25 °C at 10 K/min and equilibrated for the given time period prior to the measurement. The SAXS data were collected using a 2D multiwire gas-filled detector with pixel array dimensions of 512 × 512. The pixel size was 260 × 260 μm^2. The SAXS detector was positioned at 3 m from the sample, and the q scale was calibrated using the position of diffracted peaks from a standard silver behenate powder. The exposure time for each sample was varied from 30 to 60 s, and a wavelength of 1.24 Å was used. The WAXS data were acquired using a Photonic Science CCD camera with pixel dimension of 22 μm^2 and with a sample-to-detector distance of 95 mm. The experimental data were corrected for background scattering. The SAXS and WAXS scattered intensities were integrated after background subtraction and plotted against the scattering vector, $q = (4\pi/\lambda) \sin \theta$, where 2θ is the scattering angle.

RESULTS AND DISCUSSION

Synthesis and Macroscopic Properties. Polymers **1**−**5** were synthesized using the same batch of poly(ethylene butylene) (M_n = 3500 g/mol, PDI = 1.08) to ensure that the molecular weight and molecular weight distribution are similar for all polymers. The primary alcohol end groups of the telechelic poly(ethylene butylene) were transformed into amine end groups by a standard procedure, as previously published.[16a] The amine end groups were activated using 1,1′-carbonyldiimidazole and reacted with the corresponding UPy-C6-amine to give polymers **2**−**4**. Polymer **5** was synthesized by reaction of the corresponding isocyanate with the poly(ethylene butylene) bisamine. The newly prepared polymers **1**−**5** were purified and obtained as waxy to fibrous materials by precipitation from a chloroform solution into methanol or acetone, followed by careful washing and drying. Molecular characterization of all polymers confirmed the structures assigned and their high purity.

Table 1. Molecular Weight and Thermal Properties of Polymers 1−5

	M_n (g/mol)	PDI	T_g (°C)[b]	T_m (°C)[a]	ΔH_m (J/g)[a]	T_m (°C)[b]	ΔH_m (J/g)[b]
1	6016	1.11	−58.7	123.6; 130.0	9.332	122.5; 128.9	7.71
2	6618	1.07	−56.7	82.6; 95.7	6.98		
3	6815	1.12	−58.0	83.6	5.38		
4	6729	1.07	−57.9	81.0	0.09		
5	6430	1.13	−58.0	[c]	[c]		

[a] First heating run, 5 K/min. [b] Second heating run, 10 K/min. [c] Small cold crystallization and immediate melt was observed at 135 °C.

The thermal properties of polymers **1**−**5** were studied by DSC (Table 1). All polymers exhibited a T_g around −58 °C. In the first heating run, polymers **1** and **2** showed two distinct melting transitions. Polymers **3** and **4** both showed only one broad melting transition, where the melt transition of polymer **4** was small and hard to distinguish. Polymer **5** revealed only a small cold crystallization. None of the polymers showed any crystallization during cooling, and a clear and significant decrease in crystallinity was observed in the second heating run for all polymers. Where polymer **1** showed a rather fast recovery of the crystallinity in the second heating run, polymers **2**−**5** did not show an immediate reappearance of the melting endotherm upon reheating. Because the molecular weights of the polymers are similar, this effect cannot be caused by the viscosity of the material but should originate from the molecular differences in the UPy end groups and hence from the way they aggregate. The melting and crystallization processes are proposed to be related to the nanofiber formation (vide infra). Apparently, the nanofiber formation is highly affected by changing the substituent at the six-position of the isocytosine.

To investigate the nanofiber formation in more detail, we studied their crystallization as a function of time (Figure 2). After the first heating and cooling run, the polymers were annealed at 25 °C for an increasing amount of time after each subsequent run. In this way, the crystallinity ΔH_m could be probed as a function of time.

Polymer **1** showed almost immediate crystallization of the nanofibers. Full crystallization of the nanofibers took place within 5 h. The ratio between the two melting transitions in **1** proved to be sensitive to the cooling and heating rates.[19] For polymer **2**, full recovery of the nanofibers was obtained after 24 h, where polymer **3** took more than 3 days to crystallize and a significant lag time of several hours was observed. Polymer **4** showed hardly any crystallinity, not even after 5 days of annealing at 25 °C, whereas polymer **5** remained amorphous.

Variable temperature AFM measurements were performed on films cast from $CHCl_3$ to get more insight into the crystallization of the nanofibers (Figure 3). The AFM phase images showed a dark continuous phase representing the amorphous poly(ethylene butylene) backbone and a light, fiber-like hard domain with diameters between 6 and 7 nm originating from the aggregated UPy-urea moieties.[16a] It is not directly evident that the UPy-urea nanofibrillar hard domains are crystallized, but the regular nature of the AFM features of the polymers, together with the DSC data of these polymers, suggest that the nanofibers are crystallized. The nanofiber hard domains of polymers **1** and **2** appear more distinct and more densely packed compared with the nanofibers of polymers **3** and **4**. Polymer **4** shows a bimodal distribution of UPy-urea motifs with long nanofibers on top of a phase-separated morphology. The AFM images for polymer **1** after cooling from the melt showed the immediate recovery of the same nanofibers, whereas polymer **2** showed first a phase-separated state between the polar UPy-urea end groups and the apolar poly(ethylene butylene) backbone, as it was also observed for polymers **3** and **4**. Reappearance of the nanofibers for polymer **2** took place within 18 h. Polymer **3** showed reappearance of the fibers in 24 h. Hardly any fibers were present on the surface of **4**, not even after 11 days.

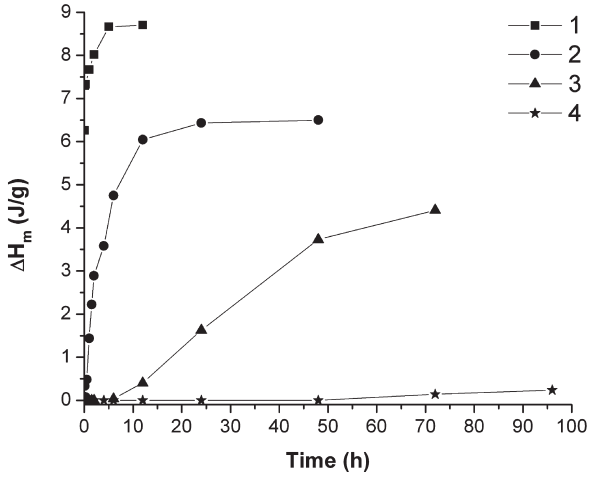

Figure 2. Crystallization of the UPy-urea nanofibers in time. (Lines are added to guide the eye.)

Both the AFM and DSC data are in agreement with the proposal that the UPy-urea end groups phase separate and crystallize into nanofibers within the apolar poly(ethylene butylene) matrix. This crystallization, however, is highly affected by the substituent at the six-position of the UPy-unit. The nanofibers show different melting points ranging from 81 to 130 °C. Crystallization of the nanofibers at 25 °C after cooling from the melt showed a remarkable dependence on the substituent on the six-position. Both the size of the substituent and the stereochemical constitution influence the rate of crystallization as well as the degree of crystallization. For polymer **4** it is almost impossible to crystallize, and the AFM images are in agreement with a phase-segregated morphology only.

To elucidate which processes are involved on the molecular scale and which one critically determines the nanofiber formation, we investigated the aggregation behavior was in more detail using the scattering techniques SAXS and WAXS and optical spectroscopy such as IR, UV−vis, and CD spectroscopy.

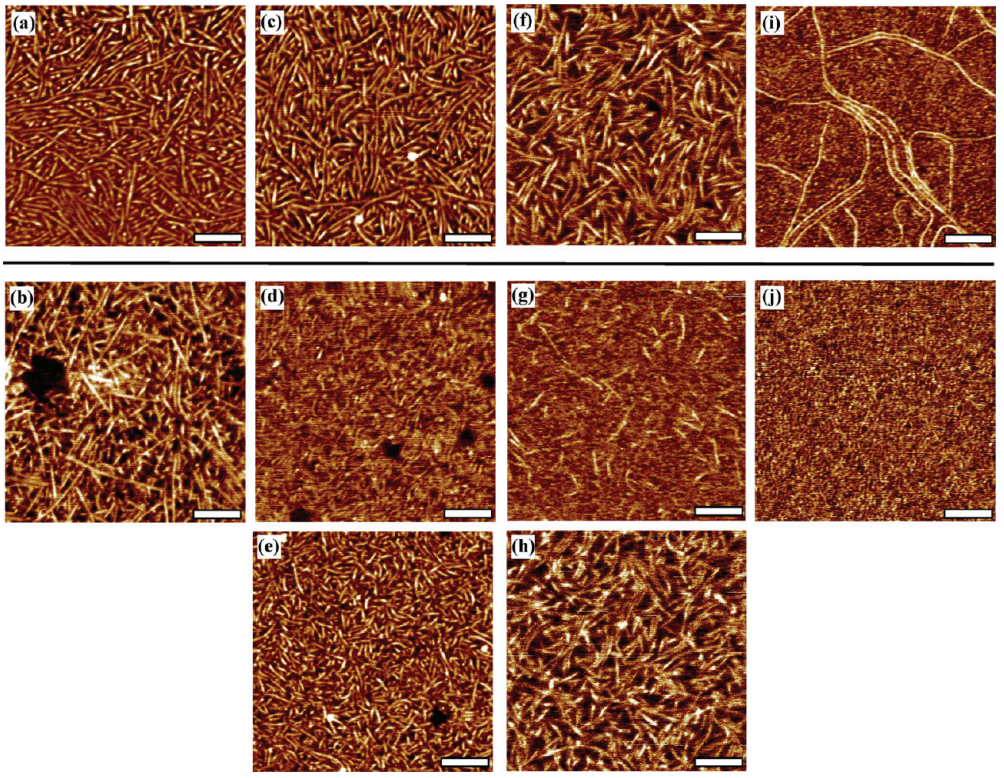

Figure 3. AFM phase images (500 × 500 nm) of polymer **1** (a) cast from $CHCl_3$ and (b) directly after cooling from the melt; polymer **2** (c) cast from $CHCl_3$ and (d) 0.6 and (e) 18 h after cooling from the melt; polymer **3** (f) cast from $CHCl_3$ and (g) 2.5 and (h) 22 h after cooling from the melt; polymer **4** (i) cast from $CHCl_3$ and (j) 2 h after cooling from the melt. Scale bar represents 100 nm.

dx.doi.org/10.1021/ma201303s |*Macromolecules* 2011, 44, 6776–6784

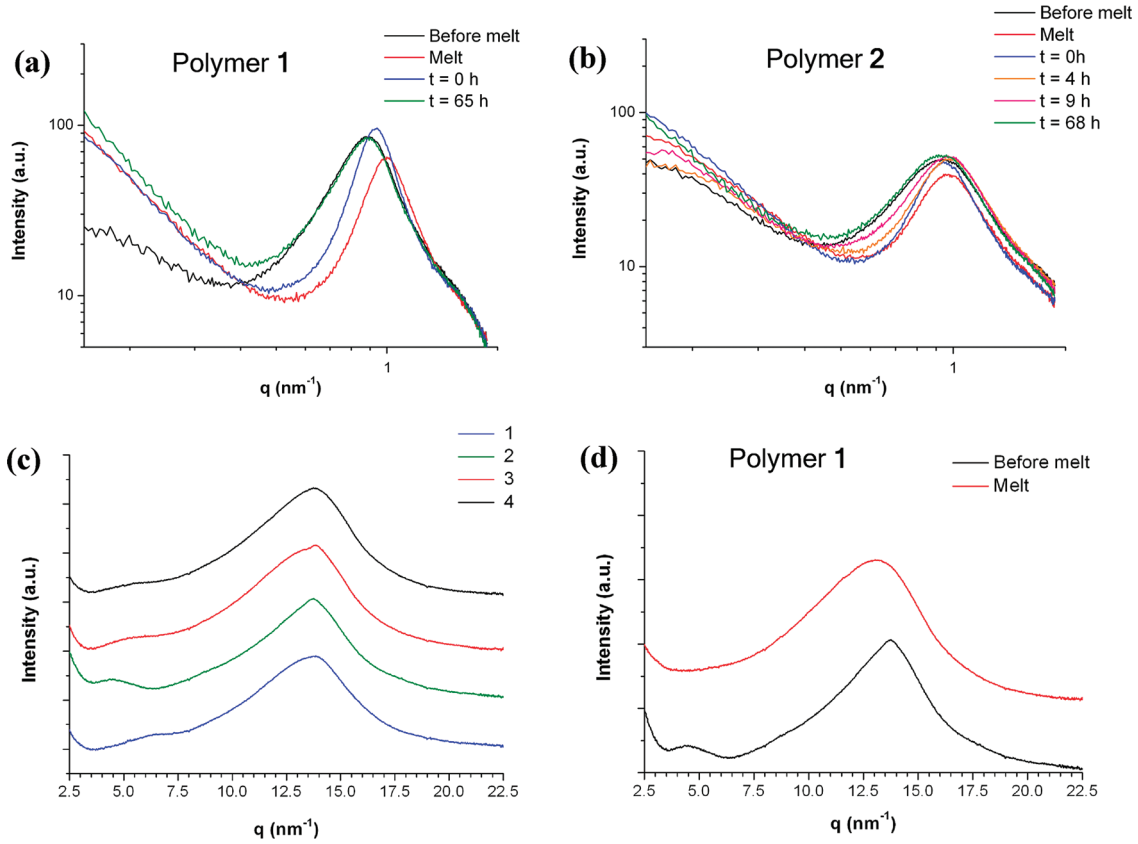

Figure 4. SAXS profiles of polymers **1** (a) and **2** (b). WAXS profiles of polymers **1**−**4** at 25 °C (c) and temperature-dependent WAXS profiles of polymer 2 (d). WAXS profiles are shifted vertically for clarity.

Table 2. X-ray Scattering Parameters Obtained for Polymers 1−4

	d spacing at 25 °C p(nm)[a]	peak half-width at 25 °C[a]	*d* spacing in melt (nm)[a]	peak half-width in melt[a]	stack-to-stack distance (nm)[b]	hydrogen bonding distance (Å)[b]
1	7.1	0.012	6.3	0.011	1.0	4.55
2	6.7	0.014	6.4	0.012	1.4	4.57
3	6.6	0.017	6.5	0.014	1.2	4.53
4	6.9	0.012[c]	6.7	0.012[c]	1.2	4.56

[a] Data derived from SAXS peak position and SAXS peak broadening. Gaussian fit. [b] Data derived from WAXS peak position. [c] Poor quality fit using a Gaussian equation. A different structural situation is possible for polymer **4**.

Molecular Scale. Temperature-dependent SAXS and WAXS studies were performed on samples of polymers **1**−**4** to reveal the ordering of the nanofibers and the order within the nanofibers, respectively. Materials of polymers **1**−**4** were obtained by cooling from the melt and were annealed at room temperature for at least 2 weeks prior to the measurements. The changes in reflections upon heating above the melt temperature and subsequent cooling were first investigated by SAXS experiments (Figure 4). In the initial spectra, a correlation peak directly related to the interfiber distance was observed in all polymers investigated (Table 2). Figure 4a shows the SAXS profiles for polymer **1**, revealing a *d* spacing of 7.1 nm before melting. Upon melting of the polymer, this correlation peak decreased in intensity and sharpened but did not disappear, indicating that phase separation occurs in the molten state. Because the polymer backbone and the UPy-urea end groups are highly different in polarity, a polar disordered phase of UPy end groups and an apolar poly(ethylene butylene) phase are likely to phase separate in the melt. Phase separation in the melt is well-documented in literature for systems like poly(ethylene butylene) block copolymers or telechelic supramolecular polymers.[20] In the melt, the SAXS correlation peak shifted to larger *q* values, correlating to shorter distances. A correlation length of ∼6.3 nm was found in the molten state of polymer **1**. Upon cooling from the melt, the correlation peak shifted back to lower *q* values. During room-temperature annealing, the SAXS peak further shifted to lower *q* values, and a clear asymmetric broadening of the peak was observed. This is an indication that objects with a larger diameter develop upon annealing, which is related to the aggregation of the UPy-urea end groups into the nanofibers. This behavior was confirmed for polymers **2** and **3**, which showed the same trend upon heating and subsequent cooling. The major difference between each polymer is the time needed for the broadening and shift to occur upon cooling, which is consistent with the different

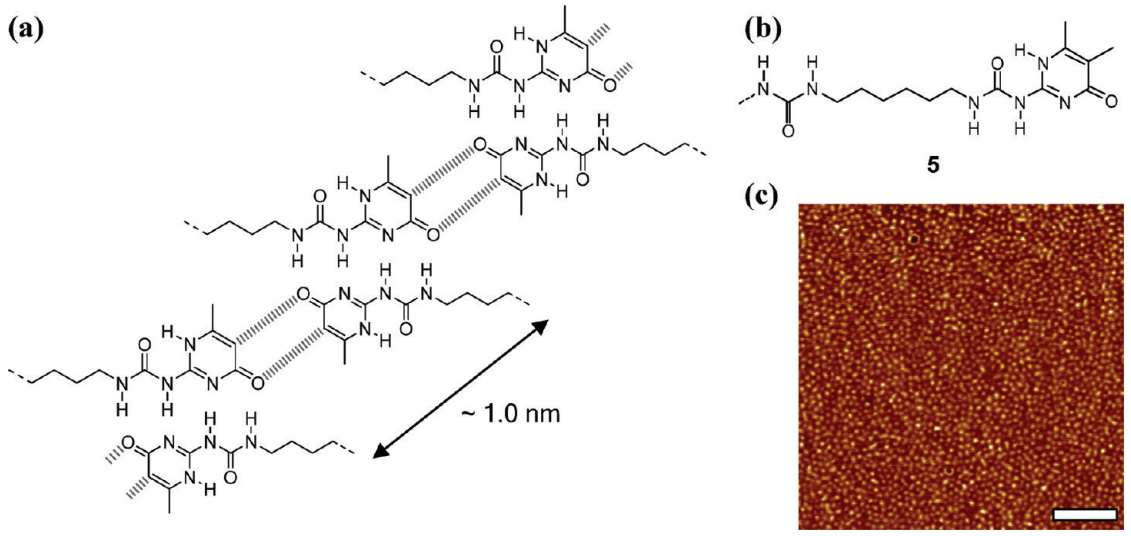

Figure 5. (a) Proposed interstack interaction, (b) 5,6-dimethyl-UPy-urea polymer **5**, and (c) AFM phase image (500 × 500 nm) of polymer **5** casted from chloroform. Scale bar represents 100 nm.

crystallization rates of the polymers previously observed by DSC measurements. Polymer **4** did not show any subsequent peak shift and peak broadening after cooling from the melt, again illustrating its hampered crystallization from the melt (Figure 4).

Information about the internal structure of the nanofibers was obtained by WAXS (Figure 4c,d). Although the WAXS profiles of all polymers were dominated by a broad halo due to the amorphous PEB structure, a weak reflection could be observed at $q \approx 13.8$ nm^{-1}. The latter corresponds to a distance of ~0.455 nm, which corresponds well with the hydrogen bonding distance found in supramolecular bisurea polymers[17a] and is therefore expected to originate from the urea hydrogen bonds. Surprisingly, a second reflection was observed corresponding to a distance of ~1 nm, which increased with increasing substituent size (Table 2). The sharpening of the WAXS reflection at $q \approx 13.8$ nm^{-1} and the reflection corresponding to a distance of ~1 nm disappeared upon melting the polymer (Figure 4d). Because the starting spectra were obtained from materials that were molten and subsequently equilibrated at room temperature for 2 weeks, these changes are thermoreversible.

The increase in distance of the 1 nm reflection upon increasing size of the substituent on the six-position prompted us to investigate the origin of this reflection. The obtained results were compared with a published single-crystal structure of a methyl-UPy derivative. (See the Supporting Information.)[18d] The in-plane neighboring UPy dimer distance of the UPy cytosine alkene proton to the pyrimidinone carboxylate of its neighboring dimer measures 1 nm (Figure 5). Recent literature describing this reflection in UPy supramolecular polymers also hints toward the existence of this interaction.[21] Other crystal structures are available that confirm the capability of cytosine alkene protons to interact intermolecularly with carbonyl moieties of neighboring cytosine molecules.[22] If the UPy dimers are stacked in polymer **1**, then this 1 nm distance corresponds to the stack-to-stack distance within an aggregated nanofiber. Because the stack-to-stack distance in the nanofibers observed with WAXS depends on the substituent type of the UPy, this substituent is expected to be placed in between the stacks. This proposal can also explain the reduced rate of crystallization of the polymers with sterically demanding substituents at the six-position.

To confirm the importance of the interstack interaction for nanofiber formation, poly(ethylene butylene) polymer **5** was studied, which has an additional methyl group at the five position of the UPy to hamper this interaction. Indeed, no nanofibers could be observed with AFM, but a phase-separated morphology was obtained (Figure 5c), which is in agreement with the lack of a melt transition in the DSC of polymer **5** (vide supra). IR spectroscopy revealed a significantly different UPy isocytosine carbonyl vibration for molecule **5** (1697 cm^{-1}) compared with polymer **1** (1702 cm^{-1}), which could suggest different hydrogen bonding of the carbonyl. This shows that the interaction of the UPy cytosine alkene proton with the pyrimidinone carboxylate of its neighboring dimer is of high importance for the nanofiber crystallization. Detailed studies on the effect of the substituent at the five position on the nanofiber formation are in progress.

Aggregation Followed by Spectroscopy. Variable temperature IR studies of the polymers in the solid phase using the reflection mode were performed to investigate the aggregation processes. Despite the fact that the UPy-motif can exist in several different tautomers, analysis at room temperature showed the 4[1*H*]-pyrimidinone tautomer to be present in all polymers, with only minor changes in the characteristic UPy vibrations (1702 and 1668 cm^{-1}) upon heating.[18d] The vibration at 1626 cm^{-1} present in the starting spectrum of polymer **1** is attributed to the strongly hydrogen-bonded urea carbonyls,[23] which shift to higher wave numbers at 140 °C. This indicates the loss of urea hydrogen bonding and hence the loss of stacking. When cooling from the melt, polymer **1** clearly showed the immediate return of the vibration at 1630 cm^{-1} (Figure 6). The small difference in frequency is attributed to a different processing history of the starting material (cast from solution) compared with the material obtained after cooling from the melt. For polymer **2**, the reappearance of the 1630 cm^{-1} vibration directly after cooling is less pronounced, whereas for polymer **3** hardly any hydrogen bonding of the urea could be observed upon cooling, although it was present in the starting spectrum. (See the Supporting Information.) For polymer **4**, no vibration corresponding to the strongly hydrogen bonded urea could be observed both before and after cooling from the melt. Apparently, urea hydrogen bonding and hence stack formation coincides with nanofiber

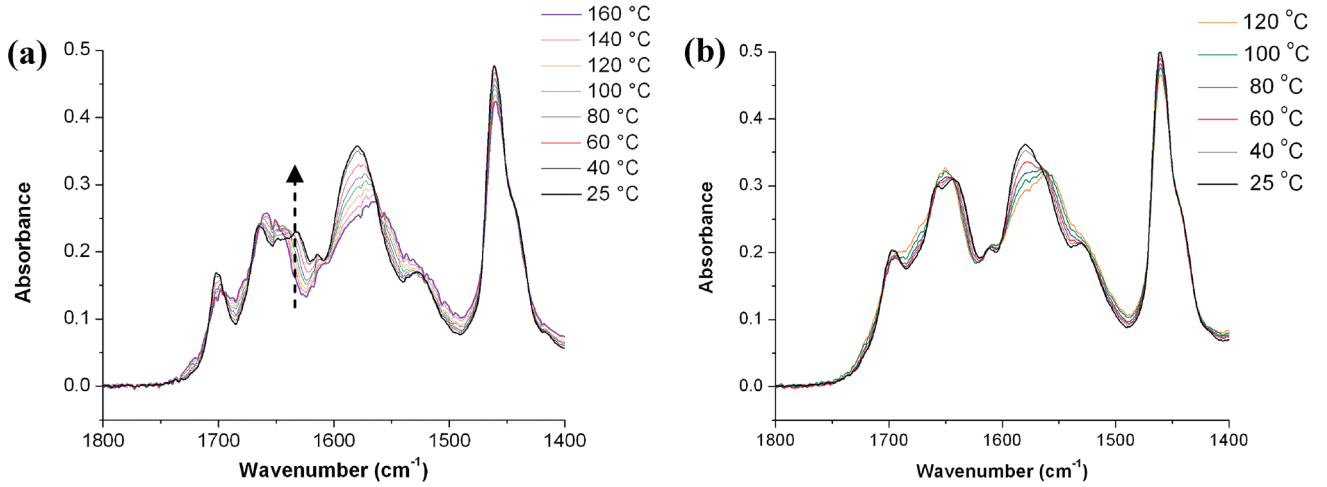

Figure 6. Infrared cooling curves of polymers **1** (a) and **3** (b) showing lateral interactions via strong urea hydrogen bonding in polymer **1** (indicated with an arrow) upon cooling from the melt.

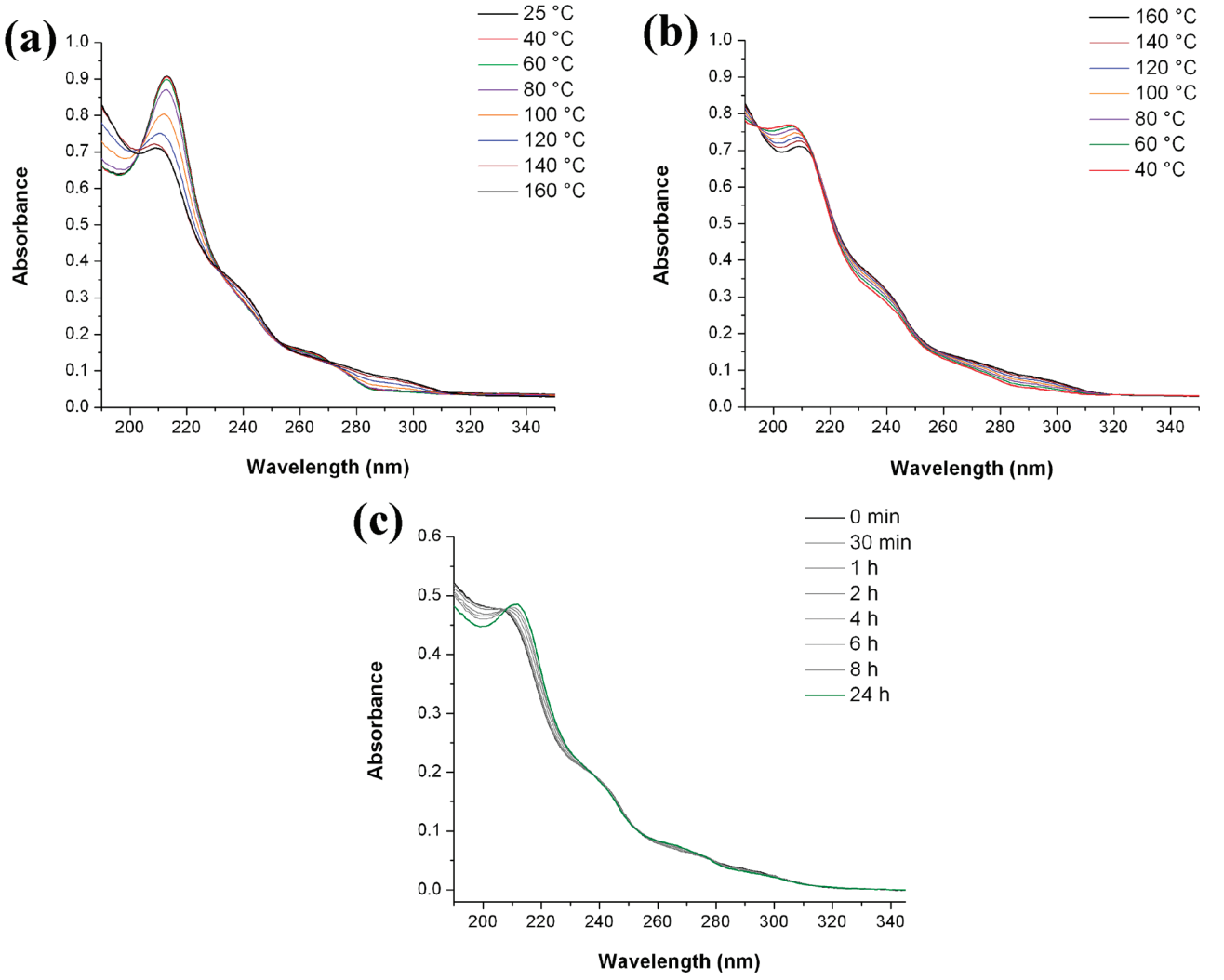

Figure 7. UV−vis spectra of polymer **2** upon melting (a), subsequent cooling (b), and annealing at 25 °C (c).

crystallization. Again, an irregular and large substituent on the UPy unit at the six-position hinders the UPy-urea motif to orient in such fashion that it allows for tight urea hydrogen bonding, which is essential for nanofiber formation.

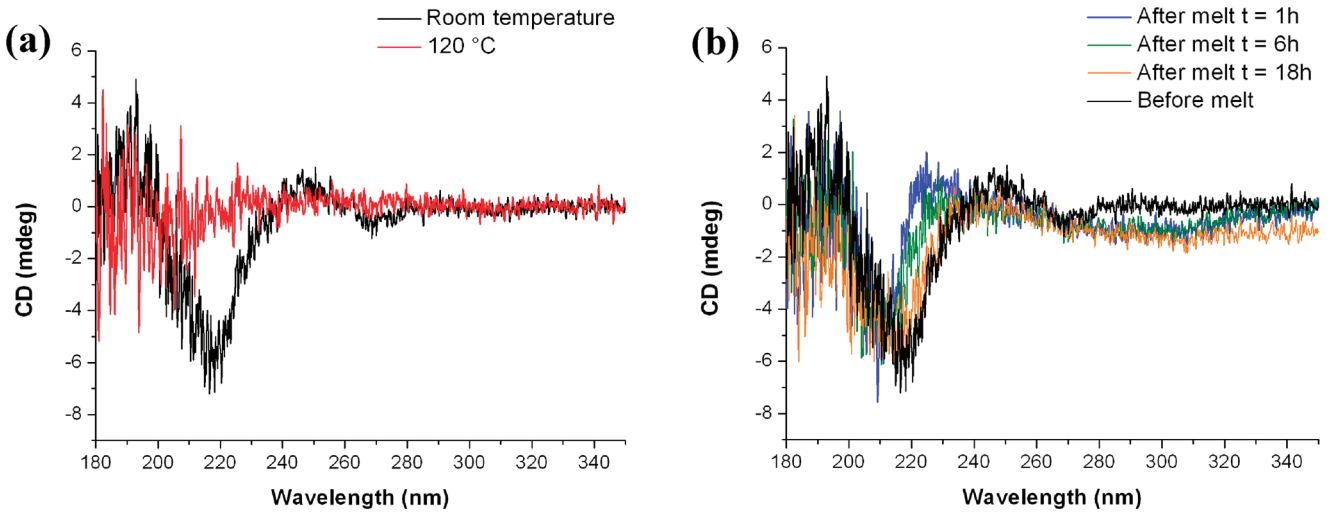

Figure 8. CD spectroscopy images of films of polymer **2** at room temperature and in the melt (a) and when annealing at room temperature after melt (b).

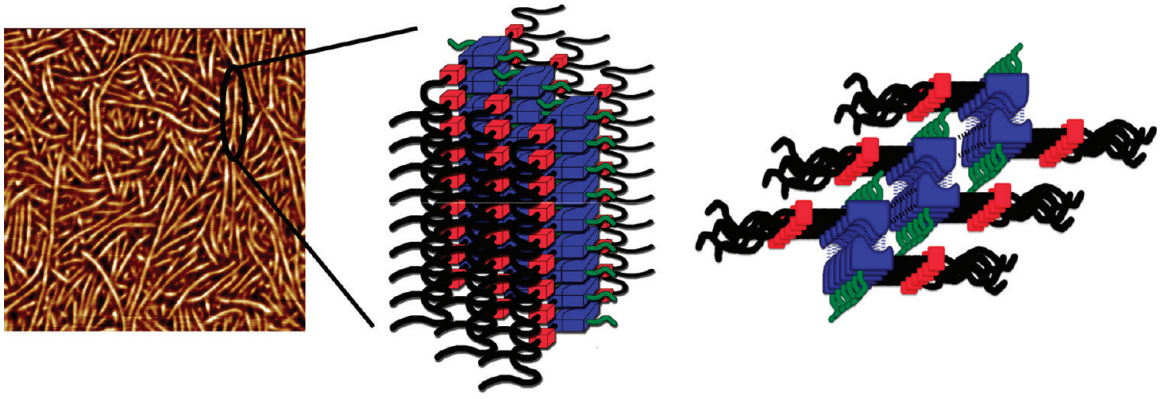

Figure 9. Schematic representation of a nanofiber. Right: Schematic top view of the nanofiber.

Finally, the optical properties of the polymers were used to study the melting and crystallization of thin polymer films. All polymers at room temperature and before melting possess the characteristic absorptions at 212 and a shoulder at 240 nm of the dimers of the UPy 4-[1H] tautomers. The absorption at 290 nm in the melt of all polymers is characteristic for the presence of the monomeric UPy 6-[1H] tautomers.[24] The reappearance of the starting UV spectrum upon cooling followed the time-dependent crystallization behavior, with blue-shifted absorptions in-between. In Figure 7, the temperature- and time-dependent UV−vis spectra of polymer **2** are presented as an example. Further details are given in the Supporting Information.

Polymers **2** and **3** are chiral because they comprise optically pure substituents. Therefore, these polymers were used to study the possible formation of aggregates with a preferred handedness. CD spectroscopy of polymer films of **2** indeed showed a Cotton effect, which disappeared upon melting of the polymer (Figure 8). Upon cooling from the melt, the Cotton effect reappeared within 1 hour. The magnitude and shape were identical but blue-shifted compared with the spectrum before melt. In time and during annealing of the film at 25 °C, the Cotton effect shifted back and returned to its original position. This fully corresponds to the behavior as observed with UV−vis spectroscopy described above. Remarkably, polymer **3** did not exhibit a Cotton effect when the films were more than 2 weeks old. Obviously, polymer **1** and **4** were CD silent. The presence of a clear Cotton effect in polymer **2** directly after cooling and before crystallization sets in suggests the presence of ordered stacks with a preferred handedness before the nanofibers are formed. The absence of a clear Cotton effect in polymer **3** can be due to the close proximity of the stereocenter (i.e., branching) to the UPy group, which may prevent stacking in a preferred handedness, thereby giving no Cotton effect.

■ CONCLUSIONS

The aggregation behavior of UPy-urea poly(ethylene butylene) telechelic polymers **1**−**4** is the result of UPy−UPy dimer formation by quadruple hydrogen bonding, lateral interactions of urea hydrogen bonds, and subsequent weak interactions between stacks, as illustrated in Figure 1. The presence of a substituent at the five-position hampers the interaction between stacks and hence nanofiber formation. The size of the substituent at the six-position determines the distance between the stacks and the rate of crystallization of the polymers upon cooling from the melt (Figure 9). The crystallization of the polymers is assigned to the formation of highly ordered nanofibers with high aspect ratios. In the nanofiber, the UPy substituent (green) is in between the UPy (blue) urea (red) stacks.

This hypothesis of structure formation in supramolecular TPEs was only possible by using a series of different analytical techniques. No single technique afforded the full picture, but they all showed the same trends in the melting and crystallization behavior. Therefore, the full picture emerged from combining parts of the puzzle obtained by the individual techniques. The exact number of stacks within a nanofiber could not be determined by any technique, but from the diameter of ~6 nm, as obtained with AFM, the maximum number of stacks can be estimated to be ~4. Whether the stacks, nanofibers, or both exhibit a helical twist could only be demonstrated with CD spectroscopy for polymer **2**. Finally, this study clearly demonstrates the subtle interplay between molecular structure and self-assembly behavior. Therefore, great care has to be taken to describe the difference of supramolecular structures formed from molecules with small molecular differences.

■ ASSOCIATED CONTENT

Supporting Information. Synthesis and characterization of polymers **1**−**5**, additional spectra, and AFM images. This material is available free of charge via the Internet at http://pubs.acs.org.

■ AUTHOR INFORMATION

Corresponding Author
*E-mail: e.w.meijer@tue.nl.

■ ACKNOWLEDGMENT

We thank the Council for Chemical Sciences of The Netherlands Organization for Scientific Research (CW-NWO) for financial support. The NWO is acknowledged for granting the beam time at the ESRF.

■ REFERENCES

(1) (a) Spontak, R. J.; Patel, N. P. *Curr. Opin. Colloid Interface Sci.* **2000**, *5*, 334–341. (b) De Rosa, C.; Auriemma, F. *Prog. Polym. Sci.* **2006**, *31*, 145–237. (c) Yilgor, I.; Yilgor, E. *Polym. Rev.* **2007**, *47*, 487–510.

(2) Armstrong, G.; Buggy, M. *J. Mater. Sci.* **2005**, *40*, 547–559.

(3) (a) Brunsveld, L.; Folmer, B. J. B.; Meijer, E. W.; Sijbesma, R. P. *Chem. Rev.* **2001**, *101*, 4071–4097. (b) Schmuck, C.; Wienand, W. *Angew. Chem., Int. Ed.* **2001**, *40*, 4363–4369.

(4) Guan, Z. *Polym. Int.* **2007**, *56*, 467–473.

(5) Cordier, Ph.; Tournilhac, F.; Soulié-Ziakovic, C.; Leibler, L. *Nature* **2008**, *451*, 977–980.

(6) (a) Folmer, B. J. B.; Sijbesma, R. P.; Versteegen, R. M.; van der Rijt, J. A. J.; Meijer, E. W. *Adv. Mater.* **2000**, *12*, 874–878. (b) Rowan, S. J.; Suwanmala, P.; Sivakova, S. *J. Polym. Sci, Part A* **2003**, *41*, 3589–3596. (c) Sivakova, S.; Bohnsack, D. A.; Mackay, M. E.; Suwanmala, P.; Rowan, S. J. *J. Am. Chem. Soc.* **2005**, *127*, 18202–18211.

(7) Sijbesma, R. P.; Beijer, F. H.; Brunsveld, L.; Folmer, B. J. B.; Hirschberg, J. H. K.; Lange, R. F. M.; Lowe, J. K. L.; Meijer, E. W. *Science* **1997**, *278*, 1601–1604.

(8) (a) Faul, C. F. J.; Antonietti, M. *Adv. Mater.* **2003**, *15*, 673–683. (b) Pollino, J. M.; Weck, M. *Chem. Soc. Rev.* **2005**, *34*, 193–207. (c) ten Brinke, G.; Ruokolainen, J.; Ikkala, O. *Adv. Polym. Sci.* **2007**, *207*, 113–177. (d) Wang, Y.; Xu, H.; Zhang, X. *Adv. Mater.* **2009**, *21*, 2849–2864. (e) Ariga, K.; Ji, Q.; Hill, J. P.; Vinu, A. *J. Inorg. Organomet. Polym.* **2010**, *20*, 1–9.

(9) Söntjens, S. H. M.; Sijbesma, R. P.; van Genderen, M. H. P.; Meijer, E. W. *J. Am. Chem. Soc.* **2000**, *122*, 7487–7493.

(10) ten Cate, A. T.; Sijbesma, R. P. *Macromol. Rapid Commun.* **2002**, *23*, 1094–1112.

(11) Yamauchi, K.; Lizotte, J. R.; Hercules, D. M.; Vergne, M. J.; Long, T. E. *J. Am. Chem. Soc.* **2002**, *124*, 8599–8604.

(12) Dankers, P. Y. W.; van Leeuwen, E. N. M.; van Gemert, G. M. L.; Spiering, A. J. H.; Harmsen, M. C.; Brouwer, L. A.; Janssen, H. M.; Bosman, A. W.; van Luyn, M. J. A.; Meijer, E. W. *Biomaterials* **2006**, *27*, 5490–5501.

(13) Dankers, P. Y. W.; Zhang, Z.; Wisse, E.; Grijpma, D. W.; Sijbesma, R. P.; Feijen, J.; Meijer, E. W. *Macromolecules* **2006**, *39*, 8763–8771.

(14) Hirschberg, J. H. K.; Beijer, F. H.; van Aert, H. A.; Magusin, P. C. M. M.; Sijbesma, R. P.; Meijer, E. W. *Macromolecules* **1999**, *32*, 2696–2705.

(15) Ligthart, G. B. W. L.; Ohkawa, H.; Sijbesma, R. P.; Meijer, E. W. *J. Am. Chem. Soc.* **2005**, *127*, 810–811.

(16) (a) Kautz, H.; van Beek, D. J. M.; Sijbesma, R. P.; Meijer, E. W. *Macromolecules* **2006**, *39*, 4265–4267. (b) Botterhuis, N. E.; van Beek, D. J. M.; van Gemert, G. M. L.; Bosman, A. W.; Sijbesma, R. P. *J. Polym. Sci, Part A* **2008**, *46*, 3877–3885.

(17) (a) Koevoets, R. A.; Versteegen, R. M.; Kooijman, H.; Spek, A. L.; Sijbesma, R. P.; Meijer, E. W. *J. Am. Chem. Soc.* **2005**, *127*, 2999–3003. (b) Versteegen, R. M.; Sijbesma, R. P.; Meijer, E. W. *Macromolecules* **2005**, *38*, 3176–3184. (c) Wisse, E.; Govaert, L. E.; Meijer, H. E. H.; Meijer, E. W. *Macromolecules* **2006**, *39*, 7425–7432. (d) Botterhuis, N. E.; Karthikeyan, S.; Veldman, D.; Meskers, S. C. J.; Sijbesma, R. P. *Chem. Commun.* **2008**, 3915–3917. (e) Botterhuis, N. E.; Karthikeyan, S.; Spiering, A. J. H.; Sijbesma, R. P. *Macromolecules* **2010**, *43*, 745–751. (f) Wisse, E.; Spiering, A. J. H.; Pfeifer, F.; Portale, G.; Siesler, H. W.; Meijer, E. W. *Macromolecules* **2009**, *42*, 524–530. (g) Sauer, B. B.; McLean, R. S.; Gaymans, R. J.; Niesten, M. C. J. E. *J. Polym. Sci, Part B* **2004**, *42*, 1783–1792. (h) De, D.; Gaymans, R. J. *Macromol. Mater. Eng.* **2009**, *294*, 405–413. (i) Wisse, E.; Spiering, A. J. H.; Dankers, P. Y. W.; Mezari, B.; Magusin, P. C. M. M.; Meijer, E. W. *J. Polym. Sci, Part A* **2011**, *49*, 1764–1771.

(18) (a) Nieuwenhuizen, M. M. L.; de Greef, T. F. A.; van der Bruggen, R. L. J.; Paulusse, J. M. J.; Appel, W. P. J.; Smulders, M. M. J.; Sijbesma, R. P.; Meijer, E. W. *Chem.—Eur. J.* **2010**, *16*, 1601–1612. (b) Alexander, A.; Bria, M.; Brunklaus, G.; Caldwell, S.; Cooke, G.; Garety, J. F.; Hewage, S. G.; Hocquel, Y.; McDonald, N.; Rabani, G.; Rosair, G.; Smith, B. O.; Spiess, H. W.; Rotello, V. M.; Woisel, P. *Chem. Commun.* **2007**, 2246–2248. (c) van Beek, D. J. M.; Spiering, A. J. H.; Peters, G. W. M.; te Nijenhuis, K.; Sijbesma, R. P. *Macromolecules* **2007**, *40*, 8464–8475. (d) Beijer, F. H.; Sijbesma, R. P.; Kooijman, H.; Spek, A. L.; Meijer, E. W. *J. Am. Chem. Soc.* **1998**, *120*, 6761–6769. (e) de Greef, T. F. A.; Ligthart, G. B. W. L.; Lutz, M.; Spek, A. L.; Meijer, E. W.; Sijbesma, R. P. *J. Am. Chem. Soc.* **2008**, *130*, 5479–5486. (f) Lafitte, V. G. H.; Aliev, A. E.; Hailes, H. C.; Bala, K.; Golding, P. *J. Org. Chem.* **2005**, *70*, 2701–2707. (h) Zhao, Y. P.; Zhao, C. C.; Wu, L. Z.; Zhang, L. P.; Tung, C. H.; Pan, Y. J. *J. Org. Chem.* **2006**, *71*, 2143–2146.

(19) The origin and thermal behavior of the two melting transitions of supramolecular polymers **1** and **2** are under investigation and will be published elsewhere.

(20) (a) Mather, B. D.; Elkins, C. L.; Beyer, F. L.; Long, T. E. *Macromol. Rapid Commun.* **2007**, *28*, 1601–1606. (b) Mather, B. D.; Baker, M. B.; Beyer, F. L.; Berg, M. A. G.; Green, M. D.; Long, T. E. *Macromolecules* **2007**, *40*, 6834–6845. (c) Nojima, S.; Kikuchi, N.; Rohadi, A.; Tanimoto, S.; Sasaki, S. *Macromolecules* **1999**, *32*, 3727–3734.

(21) Wietor, J.-L.; van Beek, D. J. M.; Peters, G. W.; Mendes, E.; Sijbesma, R. P. *Macromolecules* **2011**, *44*, 1211–1219.

(22) Lafitte, V. G. H.; Aliev, A. E.; Horton, P. N.; Hursthouse, M. B.; Bala, K.; Golding, P.; Hailes, H. C. *J. Am. Chem. Soc.* **2006**, *128*, 6544–6545.

(23) Lortie, F. L.; Boileau, S.; Bouteiller, L. *Chem.—Eur. J.* **2003**, *9*, 3008–3014.

(24) de Greef, T. F. A.; Nieuwenhuizen, M. M. L.; Sijbesma, R. P.; Meijer, E. W. *J. Org. Chem.* **2010**, *75*, 598–610.